

Anharmonic phonon behavior via irreducible derivatives: self-consistent perturbation theory and molecular dynamics

Enda Xiao¹ and Chris A. Marianetti²

¹*Department of Chemistry, Columbia University, New York, New York 10027, USA and*

²*Department of Applied Physics and Applied Mathematics,
Columbia University, New York, New York 10027, USA*

(Dated: October 28, 2022)

Cubic phonon interactions are now regularly computed from first principles, and the quartic interactions have begun to receive more attention. Given this realistic anharmonic vibrational Hamiltonian, the classical phonon Green's function can be precisely measured using molecular dynamics, which can then be used to rigorously assess the range of validity for self-consistent diagrammatic approaches in the classical limit. Here we use the bundled irreducible derivative approach to efficiently and precisely compute the cubic and quartic phonon interactions of CaF_2 , systematically obtaining the vibrational Hamiltonian purely in terms of irreducible derivatives. We assess the fidelity of various bare and self-consistent diagrammatic approaches to the phonon Green's function as compared to molecular dynamics. Specific attention is given to the phonon frequency shifts and linewidths, demonstrating that the 4-phonon bubble diagram has an important contribution to the optical phonon linewidths beyond $T = 500$ K. Moreover, accurate results are obtained even at $T = 900$ K when performing self-consistency using the 4-phonon loop diagram and evaluating the 3-phonon and 4-phonon bubble diagrams post self-consistency. This procedure of assessing the classical limit of some set of diagrams using molecular dynamics should serve as a critical test of perturbative approaches, reserving comparisons to experiment for judging the quality of the Hamiltonian itself and not the approximations used to solve it.

I. INTRODUCTION

Lattice anharmonicity is essential to the understanding of many physical properties of solids, such as thermal expansion, thermal conductivity, etc. [1]. Therefore, computing phonon interactions from first principles is a critical task. Preliminary calculations of cubic phonon interactions from first principles began decades ago using finite displacements [2], and density functional perturbation theory computations eventually followed [3, 4]. Cubic phonon interactions have since been computed in a wide range of crystals using both DFPT and finite displacements [5]. Quartic phonon interactions were investigated early on as well using finite displacements [6, 7]. While quartic phonon interactions have been formulated at the level of DFPT [3], we are not aware of any explicit calculations. Given that the number of derivatives increases drastically with the order, precisely and efficiently executing finite displacement calculations of quartic phonon interactions is critical. Recently, an approach for computing phonons and phonon interactions based on irreducible derivatives was put forward, which maximally uses group theory to reduce computational cost, and the resulting gain in efficiency can be converted into gains in accuracy [8]. Encoding anharmonicity in terms of irreducible derivatives has many advantages, including allowing a straightforward comparison between different methods. Whenever possible, it is critical to separately assess the quality of the vibrational Hamiltonian versus the solution to the vibrational Hamiltonian, as the latter will contain errors from both aspects. Here we solely focus on computing the interacting phonon Green's function of a particular realistic vibrational Hamiltonian con-

taining up to quartic phonon interactions.

The vibrational Hamiltonian poses a non-trivial many-boson problem, and therefore it is challenging to assess the quality of the method being used to solve the vibrational Hamiltonian. Imaginary time Quantum Monte-Carlo (QMC) techniques [9, 10] can be used to accurately compute thermodynamic observables for relatively large systems, and various applications exist in the literature using realistic tight-binding potentials [11, 12]. However, it is far more challenging to obtain highly accurate solutions of dynamical quantities, such as the real time phonon Green's function. Imaginary time QMC results can be approximately analytically continued to the real axis [13], but these approaches are uncontrolled and are best restricted to determining peak locations in the Green's function [14]. There are several established techniques which can be used to approximate real time quantum correlation functions [15, 16], such as centroid molecular dynamics and ring polymer molecular dynamics, but these approaches have various limitations [17] and have not yet been used to compute phonon linewidths in realistic systems; though recent studies are beginning to make average comparisons via thermal conductivity [18]. A practical approach for obtaining the Green's function on the real axis is to use diagrammatic perturbation theory, but the problem is assessing whether or not a sufficient number of diagrams have been computed. A partial solution to this problem is to revert to the classical limit where the vibrational Hamiltonian can be solved accurately using molecular dynamics, and then a perturbative solution can be rigorously assessed. Success implies that the diagrammatic approach is robust in the classical regime, and will likely be sufficient in the quantum

regime for sufficiently weak anharmonicity.

Using molecular dynamics to measure classical dynamical correlation functions is well established in the context of empirical potentials [19]. There have been a small number of studies which use an anharmonic vibrational Hamiltonian based upon first-principles calculations to measure dynamical correlation functions within MD [20–25], as is in the present study. Our MD is based purely on irreducible derivatives, which we refer to as irreducible derivative molecular dynamics (IDMD), and we have developed methods to precisely compute the irreducible derivatives from first principles [8], ensuring that we are working with a realistic vibrational Hamiltonian. A key goal of this work is to use the IDMD results to assess diagrammatic perturbation theory in the classical limit, and we are not aware of comprehensive comparisons in the existing literature.

Diagrammatic perturbation theory is a conventional method used to compute the phonon Green’s function which provides results on the real axis [26, 27]. When including up to quartic interactions in the vibrational Hamiltonian, there are four diagrams which have classical contributions up to second order in temperature [28], though only three of them are nonzero for the fluorite crystal structure [27] (see Figure 1 for a schematic and labels). The self-energy corresponding to $3b$, 4ℓ , and $4b$ is mathematically defined in equations 17, 12, and 19 of Reference [28], respectively. The imaginary part of the $3b$ self-energy is widely used in the context of perturbative thermal conductivity calculations [29, 30], and classically will provide the only contribution to the linewidth to first order in temperature. The 4ℓ diagram is purely real, and thus does not influence the phonon lifetime, and classically will provide a contribution to the phonon line shift to first order in temperature. The real part of $3b$ and 4ℓ often oppose each other [31], which justifies the success of using the bare phonon frequencies and the scattering mechanism of $3b$ in the linearized Boltzmann transport equation. The $4b$ diagram brings second order temperature dependence in the classical limit, and the imaginary part of $4b$ has been demonstrated to be important even at room temperature in select systems [32–34]. An important technical point in our work is that all diagrams are evaluated using the tetrahedron method [35], which is important to efficiently achieving convergence and removes issues associated with smearing parameters that are typically employed.

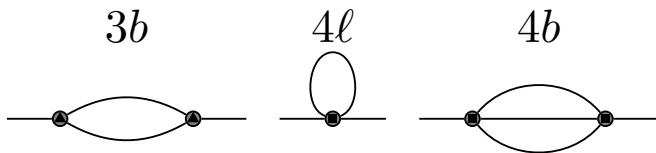


FIG. 1. A schematic of the diagrams used to construct the phonon self-energy.

Including higher order diagrams beyond $3b$, 4ℓ , and

$4b$ is cumbersome, and a more convenient approach is to perform a self-consistent perturbation theory in terms of the dressed Green’s function and skeleton diagrams [36]. Self-consistently solving Dyson’s equation using 4ℓ was initiated by Hooton from a variational perspective [37], which can be viewed as a Hartree-Fock approximation for phonons [38], and this is often referred to as the self-consistent phonon (SCP) approach or the self-consistent harmonic approximation (SCHA); though we do not use this nomenclature given that we will be executing various levels of self-consistency. The result of this approach is a real, frequency independent self-energy which renormalizes the bare phonon frequencies, though it does not produce a finite linewidth. This approach has been implemented in a small number of realistic systems in conjunction with the computation of lineshifts [39] and soft-mode driven phase transitions [40, 41]. Perhaps the simplest approach for going beyond the self-consistent 4ℓ diagram and obtaining an imaginary contribution to the self-energy is to use the resulting self-consistent 4ℓ Green’s function to evaluate the $3b$ diagram, which is known as the improved self-consistent (ISC) method [42]. This approach has been used in realistic computations of lineshifts, soft-mode driven phase transitions [43], thermal expansion [44], and thermal conductivity [39, 45].

An obvious approach for even further potential improvement would be to use the self-consistent 4ℓ Green’s function to evaluate both the $3b$ and $4b$ diagrams, which we execute in this study. Another approach is to use quasiparticle perturbation theory [46, 47] and include the real contribution of $3b$ in the self-consistency and then use the resulting Green’s function to evaluate $4b$, which we also execute in this study.

In this study we focus on the prototypical fluorite crystal CaF_2 , where we previously computed quadratic and cubic irreducible derivatives using DFT with the SCAN functional [48]. The bare $3b$ diagram was used to compute the one phonon scattering function which was then compared to inelastic neutron scattering linewidth measurements throughout the Brillouin zone at room temperature, demonstrating very good agreement. This stringent test validated the quality of our quadratic and cubic irreducible derivatives, and therefore the underlying density functional which was used to compute them, in addition to the exclusive use of the $3b$ diagram to compute the Green’s function. In the present work, we extend the Taylor series to include quartic interactions, and our goal is scrutinize a hierarchy of approximations which are used to compute the real and imaginary part of the phonon self-energy.

II. METHODOLOGY

The vibrational Hamiltonian for CaF_2 is computed from density functional theory using the lone and bundled irreducible derivative approaches (see Section III for details). Here we outline how to compute the phonon

self-energy [27], $\Sigma_{\mathbf{q}jj'}(\omega) = \Delta_{\mathbf{q}jj'}(\omega) + i\Gamma_{\mathbf{q}jj'}(\omega)$, in various approximations, which can be used to construct the phonon lineshifts and linewidths. The lowest level approximation is standard diagrammatic perturbation theory [26–28], where cubic interactions are used to construct the bubble diagram (3b) and the quartic interactions are used to construct both the bubble (4b) and the loop (4l) diagrams (see Fig. 1), resulting in

$$\Sigma_{\mathbf{q}jj'}(\omega) \approx \Sigma_{\mathbf{q}jj'}^{3b}(\omega) + \Sigma_{\mathbf{q}jj'}^{4b}(\omega) + \Sigma_{\mathbf{q}jj'}^{4l}(\omega). \quad (1)$$

The classical limit can be obtained by taking the high temperature limit of the Bose-Einstein distribution $n(\omega) \rightarrow k_B T / \hbar \omega$ and neglecting the zero-point contribution.

The next higher level of theory is self-consistent perturbation theory [36], where the dressed Green's function is used to evaluate skeleton diagrams. Self-consistent perturbation theory can be mixed with bare perturbation theory, where select diagrams are evaluated self-consistently and others are only evaluated at the end of the self-consistent process. For clarity, we introduce a notation $\Sigma_{\alpha,\beta,\dots}^{i,j,\dots}$, where i, j, \dots label diagrams that are treated self-consistently and α, β, \dots label diagrams that are evaluated using the Green's function obtained from the self-consistent process. In our notation, bare perturbation theory will not have any superscripts, the traditional self-consistent approach [37] is denoted Σ^{4l} , and the “improved” self-consistent approach [42] is denoted Σ_{3b}^{4l} . To simplify select calculations, we will also employ quasiparticle self-consistent perturbation theory [46, 47], and such calculations will have a star in the superscript. In our implementation, quasiparticle perturbation theory involves solving for the roots of $|\omega^2 - \mathbf{V}_{\mathbf{q}}(\omega)|$, where

$$V_{\mathbf{q}jj'}(\omega) = (\omega_{\mathbf{q}j}^0)^2 \delta_{jj'} + (2\omega_{\mathbf{q}j})^{\frac{1}{2}} (2\omega_{\mathbf{q}j'})^{\frac{1}{2}} \Delta_{\mathbf{q}jj'}(\omega), \quad (2)$$

$\omega_{\mathbf{q}j}^0$ is the bare phonon frequency, and $\omega_{\mathbf{q}j}$ is the renormalized phonon frequency from the previous iteration. The zeros of the preceding equation delivers the updated renormalized phonon frequencies, and the process is iterated until self-consistency is achieved. In this paper, we perform and compare the following diagrammatic calculations: $\Sigma_{4b}^{*,3b,4l}$, $\Sigma_{3b,4b}^{4l}$, Σ_{4b}^{4l} , Σ_{3b}^{4l} , Σ^{4l} , and $\Sigma_{3b,4b,4l}$.

Standard molecular dynamics approaches can be used to obtain the classical solution, which we refer to as irreducible derivative molecular dynamics (IDMD). Using the IDMD trajectory, the classical phonon spectral energy density $\mathcal{D}(\mathbf{q}, \omega)$ at reciprocal point \mathbf{q} is computed as

$$\begin{aligned} \mathcal{D}(\mathbf{q}, \omega) &= \frac{1}{2\pi N} \sum_{\mathbf{l}} e^{-i\mathbf{q} \cdot (\mathbf{l} - \mathbf{l}')} \\ &\times \sum_{dd'} \int d\tau e^{-i\omega\tau} \langle \mathbf{r}(\mathbf{l}d, \tau) \cdot \mathbf{r}(\mathbf{l}'d', 0) \rangle, \quad (3) \end{aligned}$$

where \mathbf{l} labels the lattice translation, d labels atoms within the primitive unit cell, $\mathbf{r}(\mathbf{l}d)$ is the atom displacement associate with translation \mathbf{l} and basis atom d , and

N is the number of unit cells in the crystal. The quantum $\mathcal{D}(\mathbf{q}, \omega)$ can be constructed from the quantum single particle phonon Green's function $D_{\mathbf{q}j}(\omega)$ as [27, 49]:

$$\mathcal{D}(\mathbf{q}, \omega) = \frac{\hbar n(\omega)}{2\pi} \sum_j \frac{\text{Im}(D_{\mathbf{q}j}(\omega))}{\omega_{\mathbf{q}j}^0} \sum_{dd'} \frac{\mathbf{e}_{\mathbf{q}jd} \cdot \mathbf{e}_{\mathbf{q}jd'}}{\sqrt{M_d M_{d'}}}, \quad (4)$$

where M is the mass of the nuclei, $n(\omega)$ is the Bose-Einstein distribution, and $\mathbf{e}_{\mathbf{q}jd}$ is the polarization of atom d in the mode j . The imaginary part of $D(\mathbf{q}, \omega)$ can be written in terms of the self-energy as[27]:

$$\begin{aligned} \text{Im}(D_{\mathbf{q}j}(\omega)) &= \\ &= \frac{4[\omega_{\mathbf{q}j}^0]^2 \Gamma_{\mathbf{q}jj}(\omega)}{[\omega^2 - (\omega_{\mathbf{q}j}^0)^2 - 2\omega_{\mathbf{q}j}^0 \Delta_{\mathbf{q}jj}(\omega)]^2 + [2\Gamma_{\mathbf{q}jj}(\omega) \omega_{\mathbf{q}j}^0]^2}, \quad (5) \end{aligned}$$

Equations 4 and 5 can be applied in the classical limit, allowing one to relate the numerical measurements in Eq. 3 to the classical limit of the self-energy. The simplest quasiparticle interpretation of some peak in $\mathcal{D}(\mathbf{q}, \omega)$ which is identified with $\omega_{\mathbf{q}j}^0$ can be characterized by the following trial function

$$C_0 \frac{4[\omega_{\mathbf{q}j}^0]^2 C_2}{[\omega^2 - (\omega_{\mathbf{q}j}^0)^2 - 2\omega_{\mathbf{q}j}^0 C_1]^2 + (2C_2 \omega_{\mathbf{q}j}^0)^2}, \quad (6)$$

which has three unknown coefficients C_0 , C_1 , and C_2 . For a given $\omega_{\mathbf{q}j}^0$, the corresponding peak in the IDMD measured $\mathcal{D}(\mathbf{q}, \omega)$ will be used to fit the three unknowns using linear regression. The energy window which is used to determine which data are included in the fit is 5 times the linewidth obtained from perturbation theory at the level $\Sigma_{3b,4b}$. In cases of overlapping peaks in $\mathcal{D}(\mathbf{q}, \omega)$, the corresponding peaks are individually resolved in the basis of the eigenmodes and associated with the corresponding $\omega_{\mathbf{q}j}^0$. The parameters resulting from the fitting process may be interpreted as the phonon lineshift $\Delta_{\mathbf{q}jj}(\omega_{\mathbf{q}j}^0) = C_1$ and half linewidth $\Gamma_{\mathbf{q}jj}(\omega_{\mathbf{q}j}^0) = C_2$.

III. COMPUTATIONAL DETAILS

DFT calculations within the local density approximation (LDA)[50] were performed using the projector augmented wave (PAW) method [35, 51], as implemented in the Vienna *ab initio* simulation package (VASP) [52–55]. A plane wave basis with an energy cutoff of 600 eV was employed, along with a k -point density consistent with a centered k -point mesh of $20 \times 20 \times 20$ in the primitive unit cell. All k -point integrations were done using the tetrahedron method with Blöchl corrections [35]. The DFT energies were converged to within 10^{-6} eV, while ionic relaxations were converged to within 10^{-5} eV. The structure was relaxed yielding a lattice parameter of 5.330 Å, in agreement with previous work[56]. The lattice constant is fixed in all calculations, and we do not consider thermal expansion in the present work, though it is

straightforward to incorporate the strain dependence of the irreducible derivatives [57]. The face-centered cubic lattice vectors are encoded in a 3×3 row stacked matrix $\hat{\mathbf{a}} = \frac{a_0}{2}(\hat{\mathbf{J}} - \hat{\mathbf{1}})$, where $\hat{\mathbf{1}}$ is the identity matrix and $\hat{\mathbf{J}}$ is a matrix in which each element is 1. The quadratic, cubic, and quartic irreducible derivatives were calculated via the bundled irreducible derivative (BID) approach [8]. Up to 10 finite difference discretizations were evaluated for a given measurement, such that robust error tails could be constructed and used to extrapolate to zero discretization. While the BID method only requires the absolute minimum number of measurements as required by group theory, we tripled this minimum number in order to remove the possibility of contamination due to a defective measurement. The LO-TO splitting was treated using the standard dipole-dipole approach [58, 59] and implemented using irreducible derivatives [57].

The Brillouin zone is discretized using a real space supercell $\hat{\mathbf{S}}_{BZ}\hat{\mathbf{a}}$, where $\hat{\mathbf{S}}_{BZ}$ is an invertible matrix of integers which produces superlattice vectors that satisfy the point group [8]. Two classes of supercells are used: $n\hat{\mathbf{1}}$ and $n\hat{\mathbf{S}}_O = n(4\hat{\mathbf{1}} - \hat{\mathbf{J}})$; where n is a positive integer. The second, third, and fourth order irreducible derivatives were computed for $\hat{\mathbf{S}}_{BZ} = 4\hat{\mathbf{1}}$ (containing 64 primitive cells), $\hat{\mathbf{S}}_{BZ} = \hat{\mathbf{S}}_O$ (containing 16 primitive cells), and $2\hat{\mathbf{1}}$, respectively. The quadratic and cubic irreducible derivatives have been previously computed and reported [48], and the quartic terms are reported in Supplemental Material [60].

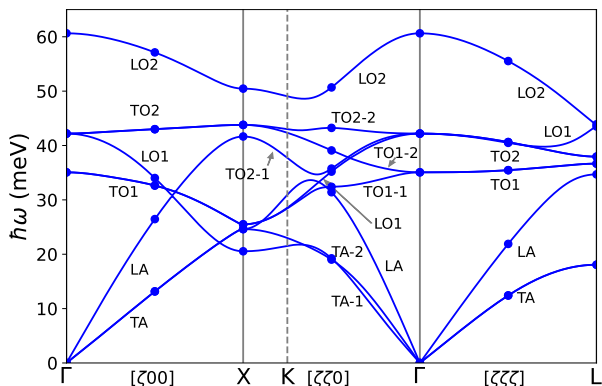


FIG. 2. The phonon dispersion of CaF_2 , including branch labels. Points are computed from DFT and lines are a Fourier interpolation.

The IDMD method is implemented using an interface to the LAMMPS[61, 62] software package. The irreducible derivatives are Fourier interpolated to a $10 \times 10 \times 10$ supercell. The Nose-Hoover thermostat [63] is used along with a 1 fs time step. For a given trajectory at each temperature, 30,000 steps are performed for initialization followed by 600,000 steps. Five trajectories are performed at each temperature, and all observables are averaged over the five trajectories. For all diagrammatic calculations, including self-consistent calcula-

tions, irreducible derivatives are Fourier interpolated to a $10 \times 10 \times 10$ supercell, and all integrations over Brillouin Zone involving the Dirac delta function are performed using the tetrahedron method[35]. The real part of the self-energy was obtained via a Kramers-Kronig transformation of the imaginary part.

IV. RESULTS AND DISCUSSION

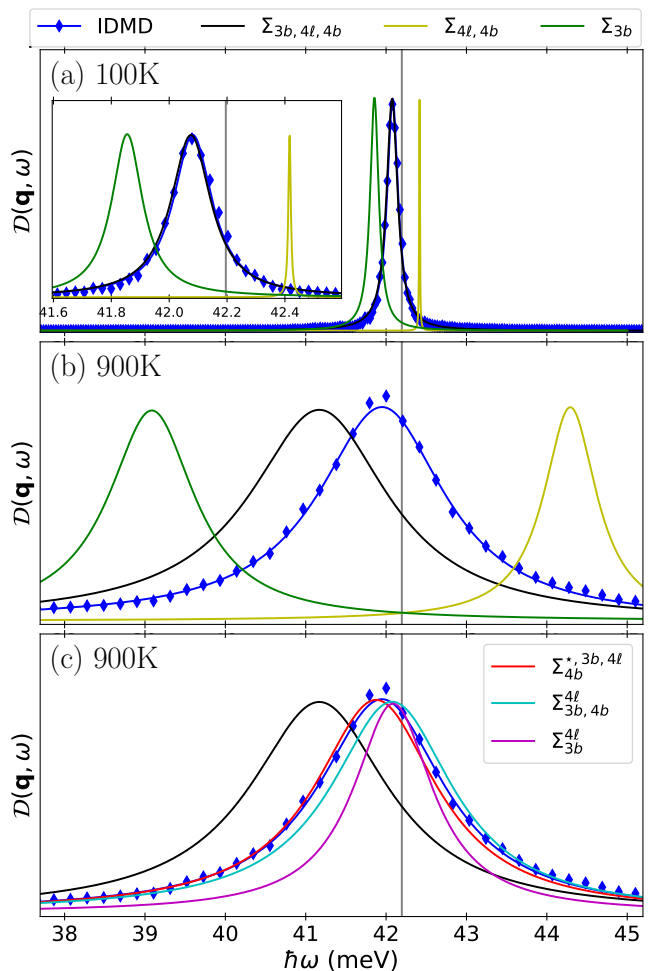


FIG. 3. Plots of $\mathcal{D}(\omega)$ at the Γ point for an energy window around the T_{2g} mode. The IDMD results are shown as blue diamonds, and the fit is shown as a blue curve. The harmonic phonon frequency is denoted as a gray vertical line. (a, b) Results at $T = 100$ K and $T = 900$ for IDMD and bare perturbation theory for various diagrams. (c) Results at $T = 900$ K for IDMD and self-consistent perturbation theory for various diagrams, in addition to $\Sigma_{3b, 4b, 4l}$. Results for Σ_{3b} and $\Sigma_{4l, 4b}$ at 100K were rescaled by 0.94 and 0.06, respectively. Results for Σ_{3b} , $\Sigma_{4l, 4b}$, $\Sigma_{3b, 4l, 4b}$, and $\Sigma_{3b, 4b}^{4l}$ at 900K were rescaled by 0.70, 0.43, 1.13, and 0.98, respectively.

We begin by examining $\mathcal{D}(\mathbf{q}, \omega)$ at the Γ -point in an energy window around the T_{2g} mode to illustrate the various methods used to solve the vibrational Hamiltonian,

which contains up to quartic terms. We will explore a low temperature and a high temperature, though a very extensive survey is provided in Supplemental Material [60]. We first consider the low temperature of $T = 100$ K, where the classical perturbative approaches should be able to reasonably describe the IDMD (see Figure 3, panel *a*). The IDMD results are shown as blue diamonds, where each point is the result of binning all measurements within a 0.02 meV window, and the blue line is the result of fitting equation 6 to the raw spectrum. We begin by comparing $\Sigma_{3b,4b,4\ell}$ to the IDMD spectra (see inset), demonstrating excellent agreement with both the line shift and width, where the former is -0.12 meV and the latter is 0.16 meV. It is interesting to further decompose the result of $\Sigma_{3b,4b,4\ell}$ into Σ_{3b} and $\Sigma_{4b,4\ell}$, demonstrating that Σ_{3b} is almost entirely responsible for the linewidth, but it also substantially shifts the mode as well. However, the shift from Σ_{3b} is partially cancelled by the shift from $\Sigma_{4b,4\ell}$, and it should be noted that the contribution from Σ_{4b} is essentially negligible at this temperature. This compensation of the shift between Σ_{3b} and $\Sigma_{4\ell}$ is not uncommon [31], and it helps justify the success of thermal conductivity calculations solely using the bare phonon frequencies and the Σ_{3b} scattering mechanism when solving the linearized Boltzmann transport equation. The satisfactory performance of bare perturbation theory implies that there is no need to consider self-consistent perturbation theory at this temperature.

We now proceed to the much higher temperature of $T = 900$ K, where the shift and width are substantially larger (see Fig 3, panel *b*). As in the low temperature case, Σ_{3b} causes a downward shift and generates a non-trivial linewidth. Unlike the low temperature case, $\Sigma_{4b,4\ell}$ not only shifts the peak upward, but also generates a substantial linewidth. Given that $\Sigma_{4\ell}$ is purely real, all of the linewidth contribution of $\Sigma_{4b,4\ell}$ arises from Σ_{4b} , demonstrating that Σ_{4b} can be an important contribution to the imaginary part of the self-energy at higher temperatures. Taking all contributions together, the $\Sigma_{3b,4b,4\ell}$ provides a reasonable description of the IDMD result, though there is a clear error in the shift, which suggests that self-consistent perturbation theory may be needed. Indeed, $\Sigma_{4b}^{*,3b,4\ell}$ provides an excellent description of the IDMD results (see Fig 3, panel *c*). When moving down one level to $\Sigma_{3b,4b}^{4\ell}$, the only notable degradation of the result is a small shift to higher frequencies. It is also interesting to consider $\Sigma_{3b}^{4\ell}$, which is also referred to as the ISC, which shows a substantial error in the linewidth.

The preceding analysis carefully explored the results of different diagrams for a single mode, and we now proceed to survey select branches throughout the Brillouin zone. We begin by examining the phonon line shift and width of the TA-2 and TO2-2 modes at $T = 100$ K (see Figure 4). For both the line shifts and widths, the $\Sigma_{3b,4b,4\ell}$ result yields results that are close to the IDMD. There are some regions where small differences can be noted, and care must be taken when scrutinizing the results given the overall small magnitude of the numbers

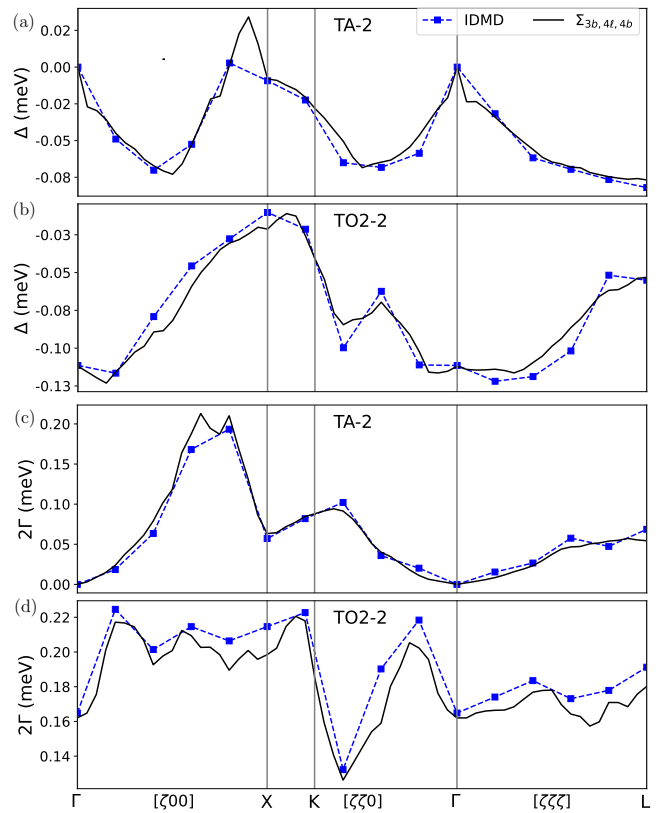


FIG. 4. Phonon lineshifts (*a*, *b*) and linewidths (*c*, *d*) of the TA-2 (*a*, *c*) and TO2-2 (*b*, *d*) modes at $T = 100$ K along various paths through the Brillouin zone. IDMD and $\Sigma_{3b,4b,4\ell}$ results are blue squares and black curves, respectively. Dashed curves are guides to the eye.

at hand. Nonetheless, the differences mostly appear to arise from higher order diagrams, given that including self-consistency mostly tends to move the diagrammatic solution closer to the IDMD [60].

Having established the fidelity of our diagrammatic approaches and IDMD at low temperatures, we now proceed to the high temperature of $T = 900$ K where IDMD can be used to judge the accuracy of different levels of bare and self-consistent perturbation theory (see Figure 5). As done previously, we explore the TA-2 and TO2-2 modes, but here we consider self-consistent perturbation theory as well given the deficiency of bare perturbation theory at this temperature. We begin by examining the shift of the TA-2 mode (panel *a*), where $\Sigma_{3b,4b,4\ell}$ yields good results in certain portions of the zone, but performs poorly in selected regions. Including self-consistency via $\Sigma_{4b}^{*,3b,4\ell}$ and $\Sigma_{3b,4b}^{4\ell}$ tends to correct large deviations that are observed in $\Sigma_{3b,4b,4\ell}$. For the shift of the TO2-2 modes (panel *b*), the $\Sigma_{3b,4b,4\ell}$ result yields a more systematic error, where the results are shifted in a nearly uniform manner, and the result even has the wrong sign in some cases. In this case, $\Sigma_{3b,4b}^{4\ell}$ offers a drastic improvement, and $\Sigma_{4b}^{*,3b,4\ell}$ pushes the result even closer to IDMD. The linewidths have similar behavior to the

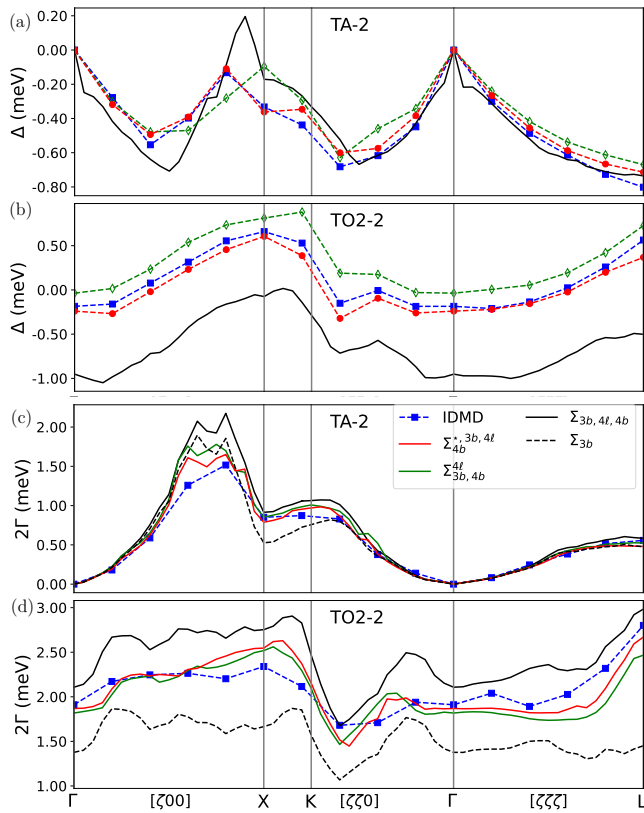


FIG. 5. Phonon lineshifts (a, b) and linewidths (c, d) of the TA-2 (a, c) and TO2-2 (b, d) modes at $T = 900$ K along various paths through the Brillouin zone. IDMD, $\Sigma_{4b}^{*,3b,4l}$, $\Sigma_{3b,4b}^{4l}$, $\Sigma_{3b,4b,4l}$, and Σ_{3b} results are blue squares, red curves, green curves, black curves, and dashed black curves, respectively. Dashed blue curves are guides to the eye.

lineshifts in the two respective cases (see panels c and d). In the case of TA-2, it is interesting to consider Σ_{3b} , given its importance in the context of common treatments of thermal conductivity, and it is clear that it yields remarkable results. However, Σ_{3b} performs poorly for the TO2-2 modes. The general trends that we have outlined here can also be seen in other modes, and comprehensive results for all branches at temperatures of 100K, 300K, 500K, 700K, and 900K are included in Supplemental Material [60]. We also provide a corresponding analysis where all cubic interactions are set to zero [60].

V. CONCLUSION

In summary, we have computed the irreducible derivatives of CaF_2 up to fourth order, defining the vibrational Hamiltonian. We use molecular dynamics to solve the vibrational Hamiltonian, which we refer to as irreducible derivative molecular dynamics (IDMD), yielding the real and imaginary part of the phonon self-energy in the classical limit. The IDMD result was then used as a benchmark for various levels of diagrammatic perturbation the-

ory. At the low temperature of $T = 100$ K, we show that bare perturbation performs well using the $3b$, $4l$, and $4b$ diagrams (i.e. $\Sigma_{3b,4l,4b}$). While the linewidth is reasonably well described by $3b$ alone, $4l$ is also necessary to properly capture the lineshift. At the high temperature of $T = 900$ K, bare perturbation theory only performs well for the linewidths of the acoustic modes, where even $3b$ alone yields reasonable results. Treating the $4l$ diagram self-consistently and evaluating $3b$ and $4b$ post self-consistency (i.e. $\Sigma_{3b,4b}^{4l}$) is critical to obtaining accurate lineshifts for all branches, in addition to obtaining accurate linewidths for the optical modes. Further improvement is normally obtained when performing quasiparticle self-consistent perturbation theory, where the real part of the $3b$ diagram is used during self-consistency (i.e. $\Sigma_{4b}^{*,3b,4l}$).

The procedure outlined in this paper of assessing various levels of diagrammatic perturbation theory in the classical limit using molecular dynamics should be viable on nearly any system where the Taylor series can be constructed. Once some class of diagrams is validated classically, it is likely that the quantum counterparts will also perform well at lower temperatures in the quantum regime so long as the anharmonicity is sufficiently weak. Furthermore, the prescribed diagrams may be combined with other diagrammatic approaches to scattering, such as defects or electron-phonon coupling in the case of metals. An obvious application of the philosophy of this paper would be phonon mediated thermal conductivity, where the molecular dynamics solution would yield the thermal conductivity within Kubo-Green linear response, and various levels of self-consistent diagrammatic perturbation theory could be tested in conjunction with the linearized Boltzmann transport equation in the classical limit.

VI. ACKNOWLEDGEMENTS

This work was supported by the grant DE-SC0016507 funded by the U.S. Department of Energy, Office of Science. This research used resources of the National Energy Research Scientific Computing Center, a DOE Office of Science User Facility supported by the Office of Science of the U.S. Department of Energy under Contract No. DE-AC02-05CH11231.

- [1] D. Wallace, *Thermodynamics of Crystals* (Dover, 1998).
- [2] H. Wendel and R. M. Martin, Phys. Rev. Lett. **40**, 950 (1978).
- [3] X. Gonze, Physical Review A **52**, 1096 (1995).
- [4] A. Debernardi, S. Baroni, and E. Molinari, Phys. Rev. Lett. **75**, 1819 (1995).
- [5] L. Lindsay, A. Katre, A. Cepellotti, and N. Mingo, Journal Of Applied Physics **126**, 050902 (2019).
- [6] D. Vanderbilt, S. H. Taole, and S. Narasimhan, Phys. Rev. B **40**, 5657 (1989).
- [7] S. Narasimhan and D. Vanderbilt, Phys. Rev. B **43**, 4541 (1991).
- [8] L. Fu, M. Kornbluth, Z. Cheng, and C. A. Marianetti, Phys. Rev. B **100**, 014303 (2019), publisher: American Physical Society.
- [9] D. M. Ceperley, Rev. Mod. Phys. **67**, 279 (1995).
- [10] D. M. Ceperley, Rev. Mod. Phys. **71**, 438 (1999).
- [11] R. Ramirez, C. P. Herrero, and E. R. Hernandez, Phys. Rev. B **73**, 245202 (2006).
- [12] R. Ramirez, C. P. Herrero, E. R. Hernandez, and M. Cardona, Phys. Rev. B **77**, 045210 (2008).
- [13] M. Jarrell and J. E. Gubernatis, Physics Reports-review Section Of Physics Letters **269**, 133 (1996).
- [14] V. Sorkin, E. Polturak, and J. Adler, Phys. Rev. B **71**, 214304 (2005).
- [15] A. Perez, M. E. Tuckerman, and M. H. Muser, Journal Of Chemical Physics **130**, 184105 (2009).
- [16] S. C. Althorpe, European Physical Journal B **94**, 155 (2021).
- [17] S. Habershon, D. E. Manolopoulos, T. E. Markland, and T. F. Miller, Annual Review Of Physical Chemistry, Vol 64 Se Annual Review Of Physical Chemistry **64**, 387 (2013).
- [18] R. P. Luo and K. Yu, Journal Of Chemical Physics **153**, 194105 (2020).
- [19] C. Z. Wang, C. T. Chan, and K. M. Ho, Phys. Rev. B **42**, 11276 (1990), publisher: American Physical Society.
- [20] A. Glensk, B. Grabowski, T. Hickel, J. Neugebauer, J. Neuhaus, K. Hradil, W. Petry, and M. Leitner, Phys. Rev. Lett. **123**, 235501 (2019).
- [21] K. Esfarjani, G. Chen, and H. T. Stokes, Phys. Rev. B **84**, 085204 (2011).
- [22] J. Shiomi, K. Esfarjani, and G. Chen, Phys. Rev. B **84**, 104302 (2011), publisher: American Physical Society.
- [23] T. Murakami, T. Shiga, T. Hori, K. Esfarjani, and J. Shiomi, EPL **102**, 46002 (2013), publisher: IOP Publishing.
- [24] T. Shiga, T. Murakami, T. Hori, O. Delaire, and J. Shiomi, Appl. Phys. Express **7**, 041801 (2014), publisher: IOP Publishing.
- [25] F. Zhou, W. Nielson, Y. Xia, and V. Ozoliņš, Phys. Rev. B **100**, 184308 (2019).
- [26] J. J. Kokkedee, Physica **28**, 374 (1962).
- [27] A. A. Maradudin and A. E. Fein, Phys. Rev. **128**, 2589 (1962).
- [28] R. S. Tripathi and K. N. Pathak, Nuov Cim B **21**, 289 (1974).
- [29] D. A. Broido, M. Malorny, G. Birner, N. Mingo, and D. A. Stewart, Appl. Phys. Lett. **91**, 231922 (2007), publisher: American Institute of Physics.
- [30] L. Lindsay, C. Hua, X. L. Ruan, and S. Lee, Materials Today Physics **7**, 106 (2018).
- [31] M. Lazzeri, M. Calandra, and F. Mauri, Phys. Rev. B **68**, 220509 (2003).
- [32] J. S. Kang, M. Li, H. A. Wu, H. Nguyen, and Y. J. Hu, Science **361**, 575 (2018).
- [33] F. Tian, B. Song, X. Chen, N. K. Ravichandran, Y. C. Lv, K. Chen, S. Sullivan, J. Kim, Y. Y. Zhou, T. H. Liu, M. Goni, Z. W. Ding, J. Y. Sun, G. Gamage, H. R. Sun, H. Ziyae, S. Y. Huyan, L. Z. Deng, J. S. Zhou, A. J. Schmidt, S. Chen, C. W. Chu, P. Huang, D. Broido, L. Shi, G. Chen, and Z. F. Ren, Science **361**, 582 (2018).
- [34] S. Li, Q. Y. Zheng, Y. C. Lv, X. Y. Liu, X. Q. Wang, P. Huang, D. G. Cahill, and B. Lv, Science **361**, 579 (2018).
- [35] P. E. Blöchl, O. Jepsen, and O. K. Andersen, Phys. Rev. B **49**, 16223 (1994).
- [36] R. M. Martin, L. Reining, and D. M. Ceperley, *Interacting Electrons: Theory and Computational Approaches*, 1st ed. (Cambridge University Press, 2016).
- [37] D. Hooton, The London, Edinburgh, and Dublin Philosophical Magazine and Journal of Science **46**, 422 (1955), publisher: Taylor & Francis eprint: <https://doi.org/10.1080/14786440408520575>.
- [38] W. Jones and N. H. March, *Theoretical Solid State Physics, Volume 1: Perfect Lattices in Equilibrium* (Dover Publications, New York, 2011).
- [39] T. Tadano and S. Tsuneyuki, Phys. Rev. B **92**, 10.1103/PhysRevB.92.054301 (2015), publisher: American Physical Society.
- [40] I. Errea, B. Rousseau, and A. Bergara, Phys. Rev. Lett. **106**, 165501 (2011), publisher: American Physical Society.
- [41] R. Bianco, I. Errea, L. Paulatto, M. Calandra, and F. Mauri, Phys. Rev. B **96**, 014111 (2017).
- [42] V. V. Goldman, G. K. Horton, and M. L. Klein, Phys. Rev. Lett. **21**, 1527 (1968), publisher: American Physical Society.
- [43] R. Masuki, T. Nomoto, R. Arita, and T. Tadano, (2022), arXiv:2205.08789 [cond-mat].
- [44] Y. Oba, T. Tadano, R. Akashi, and S. Tsuneyuki, Phys. Rev. Materials **3**, 033601 (2019), publisher: American Physical Society.
- [45] T. Tadano and S. Tsuneyuki, Phys. Rev. Lett. **120**, 105901 (2018), publisher: American Physical Society.
- [46] S. V. Faleev, M. van Schilfgaarde, and T. Kotani, Phys. Rev. Lett. **93**, 126406 (2004).
- [47] M. van Schilfgaarde, T. Kotani, and S. Faleev, Phys. Rev. Lett. **96**, 226402 (2006).
- [48] E. Xiao, H. Ma, M. S. Bryan, L. Fu, J. M. Mann, B. Winn, D. L. Abernathy, R. P. Hermann, A. R. Khanolkar, C. A. Dennett, D. H. Hurley, M. E. Manley, and C. A. Marianetti, Phys. Rev. B **106**, 144310 (2022).
- [49] G. L. Squires, *Introduction to the Theory of Thermal Neutron Scattering*, 3rd ed. (Cambridge University Press, 2012).
- [50] J. P. Perdew and A. Zunger, Phys. Rev. B **23**, 5048 (1981).
- [51] G. Kresse and D. Joubert, Phys. Rev. B **59**, 1758 (1999).
- [52] G. Kresse and J. Hafner, Phys. Rev. B **47**, 558 (1993).
- [53] G. Kresse and J. Hafner, Phys. Rev. B **49**, 14251 (1994).
- [54] G. Kresse and J. Furthmuller, Computational Materials Science **6**, 15 (1996).
- [55] G. Kresse and J. Furthmuller, Phys. Rev. B **54**, 11169 (1996).
- [56] K. Schmalzl, D. Strauch, H. Schober, B. Dorner, and A. Ivanov, in *High Performance Computing in Science and Engineering, Munich 2002*, edited by S. Wagner, A. Bode, W. Hanke, and F. Durst (Springer Berlin Heidelberg, Berlin,

- Heidelberg, 2003) pp. 249–258.
- [57] M. A. Mathis, A. Khanolkar, L. Fu, M. S. Bryan, C. A. Dennett, K. Rickert, J. M. Mann, B. Winn, D. L. Abernathy, M. E. Manley, D. H. Hurley, and C. A. Marianetti, *Phys. Rev. B* **106**, 014314 (2022).
- [58] X. Gonze and C. Lee, *Phys. Rev. B* **55**, 10355 (1997).
- [59] P. Giannozzi, S. D. Gironcoli, P. Pavone, and S. Baroni, *Phys. Rev. B* **43**, 7231 (1991).
- [60] See Supplemental Material at [URL will be inserted by publisher] for shift and linewidth for all branches from 100K to 900K, decomposition of $\Sigma_{3b,4\ell,4b}$ to Σ_{3b} , $\Sigma_{4\ell}$, and Σ_{4b} , and irreducible derivatives.
- [61] A. P. Thompson, H. M. Aktulga, R. Berger, D. S. Bolintineanu, W. M. Brown, P. S. Crozier, P. J. in 't Veld, A. Kohlmeyer, S. G. Moore, T. D. Nguyen, R. Shan, M. J. Stevens, J. Tranchida, C. Trott, and S. J. Plimpton, *Comp. Phys. Comm.* **271**, 108171 (2022).
- [62] S. Plimpton, *Journal of Computational Physics* **117**, 1 (1995).
- [63] S. Nosé, *J. Chem. Phys.* **81**, 511 (1984), publisher: American Institute of Physics.